Diamond & Related Materials 116 (2021) 108394

Contents lists available at ScienceDirect

Diamond & Related Materials

journal homepage: www.elsevier.com/locate/diamond

Large area microwave plasma CVD of diamond using composite right/left-handed materials

Justas Zalieckas [a,*], Paulius Pobedinskas [b,c], Martin Møller Greve [a], Kristoffer Eikehaug [a], Ken Haenen [b,c], Bodil Holst [a]

[a] Department of Physics and Technology, University of Bergen, Allegaten 55, Bergen, Norway
[b] Institute for Materials Research (IMO), Hasselt University, Wetenschapspark 1, 3590 Diepenbeek, Belgium
[c] IMOMEC, IMEC vzw, Wetenschapspark 1, 3590 Diepenbeek, Belgium

ARTICLE INFO

Keywords:
Large area diamond CVD
Right/left-handed materials
Nanocrystalline diamond
Surface wave plasma

ABSTRACT

Diamond growth at low temperatures ($\leq$400 °C) and over large areas is attractive for materials, which are sensitive to high temperatures and require good electronic, chemical or surface tribological properties. Resonant-cavity microwave plasma enhanced (MWPE) chemical vapor deposition (CVD) is a standard method for growing diamonds, however, with limited deposition area. An alternative method for CVD of diamond over large area and at low temperature is to use a surface wave plasma (SWP). In this work we introduce a novel method to excite SWP using composite right/left-handed (CRLH) materials and demonstrate growth of nanocrystalline diamond (NCD) on 4-inch Si wafers. The method uses a set of slotted CRLH waveguides coupled to a resonant launcher, which is connected to a deposition chamber. Each CRLH waveguide supports infinite wavelength propagation and consists of a chain of periodically cascaded unit cells. The SWP is excited by a set of slots placed to interrupt large area surface current on the resonant launcher. This configuration yields a uniform gas discharge distribution. We achieve 80 nm/h growth rate for NCD films with a low surface roughness (5–10 nm) at 395 °C and 0.5 mbar pressure using a $H_2/CH_4/CO_2$ gas mixture.

1. Introduction

Nanocrystalline diamond (NCD) with excellent physical, chemical and surface tribological properties is an attractive material for micro-electro-mechanical systems, biosensors, thermal management and applications requiring high abrasion resistance [1–4]. Most of these applications demand uniform diamond films over large areas, which is a major challenge for industry and the research community. The two most widely used methods for growing NCD are hot filament (HF) and microwave plasma enhanced (MWPE) chemical vapor deposition (CVD).

The HFCVD is a preferred method in industry for a large area CVD due to a relatively low cost and scalability. The scalability is achieved by extending or adding more filaments that can yield deposition areas of up to few square meters. The HFCVD method, however, suffers from two main drawbacks: long-term filament instability and contamination of the growing diamond film by metal evaporation from the filament itself. The long-term filament instability is a result of the filament corrosion and formation of carbides on the filament during the incubation period and CVD process. This can lead to filament distortion thus altering NCD growth conditions [5,6]. Therefore, for the growth of high purity diamond films, typically, resonant-cavity MWPECVD systems operating at 2.45 GHz frequency are used. The deposition area of these systems is limited by the gas discharge shape and size, which is roughly half the wavelength at a given frequency. The limited scaling-up of the gas discharge size can be achieved by lowering MW generator frequency from 2.45 GHz to 915 MHz, yielding deposition areas of up to approximately 30 cm^2 and 200 cm^2, respectively. It is worth noting, however, that lowering generator frequency reduces MW power density by a factor of two leading to higher operational costs [7].

Diamond films, typically, are grown at substrate temperatures ranging from 500 °C to 1000 °C in HFCVD and resonant-cavity MWPECVD systems [8]. Such high substrate temperatures limit the range of substrate materials, which can be used for diamond synthesis. It is worth noting, however, that multiple research groups have succeeded growing diamond at low substrate temperatures ($\leq$400 °C) reaching 135 °C with HFCVD [9,10], 350 °C with MWPECVD [11–14], and 200 °C

* Corresponding author.
E-mail address: justas.zalieckas@uib.no (J. Zalieckas).

https://doi.org/10.1016/j.diamond.2021.108394
Received 3 March 2021; Received in revised form 28 March 2021; Accepted 29 March 2021
Available online 10 April 2021

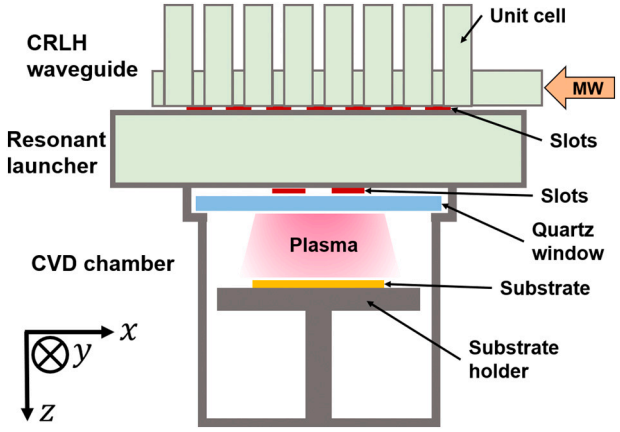

Fig. 1. Schematic drawing of the new SWP MWPECVD system consisting of the CRLH waveguides, the resonant launcher and the CVD chamber.

using magneto-active plasma CVD method [15]. As an alternative to HFCVD and resonant-cavity MWPECVD either a distributed antenna array (DAA) [16,17] or a surface wave plasma (SWP) [18–21] MWPECVD system could be used to mitigate above mentioned drawbacks. The SWP and DAA systems can achieve large area and uniform diamond CVD at low temperatures ($\leq$400 $^{\circ}C$) using a $H_2/CH_4/CO_2$ gas mixture, which is desirable for diamond synthesis on substrates sensitive to high temperatures such as plastic. NCD films have been successfully synthesized on plastic at substrate temperatures below 100 $^{\circ}C$ using SWP method [22]. Furthermore, growth at low temperature reduces the stress induced by the mismatch of coefficients of thermal expansion between the substrate and the film.

The DAA system is based on multiple elementary microwave plasma sources arranged in a square lattice matrix configuration [23]. The MW power to each plasma source is distributed via waveguide-based power divider followed by a matching circuit comprising a tuning means and a ferrite isolator [24]. Therefore, scalability of DAA microwave system introduces additional complexity and cost. SWP, on the other hand, can be excited by linear [25] and slotted [19] antennas or different types of microwave launchers [26–28]. Linear antenna SWP is excited by a set of coaxial linear antennas each surrounded by a quartz tube [29–31]. The low directivity of the linear antenna yields inefficient MW radiation distribution towards the deposition area. Additionally, a standing electromagnetic wave is formed along each antenna thus affecting the uniformity of the electric field and plasma distributions. The SWP excited by slotted antennas suffers from problems such as arc discharges, heating of the dielectric window and localized plasmas around the slots yielding non-uniform plasma density. Various configurations of advanced-geometry slotted antennas were proposed to mitigate these effects [19,32]. However, the fundamental limit in the slot-based approach is the constraint on minimum distance between two adjacent slots (d_s). The d_s is determined by the waveguide surface current distribution and is given by half of the waveguide wavelength ($d_s = \lambda_g/2$) [33].

In this work we introduce a new method to excite SWP that uses the unique properties of metamaterials. Composite right/left-handed (CRLH) materials [34] with infinite wavelength propagation property are used to achieve $d_s < \lambda_g/2$. We have designed and built the new SWP MWPECVD system based on 3D numerical electromagnetic field simulations and experimentally realized growth of a smooth NCD film on 4-inch Si wafers.

2. Numerical simulations

The SWP MWPECVD system operates at 2.465 GHz frequency and consists of three interconnected parts: an array of CRLH waveguides, a resonant launcher and a CVD chamber. Fig. 1 shows a schematic drawing of the system. The slotted CRLH waveguides work at infinite wavelength propagation frequency and are coupled to the resonant launcher. The surface current on the resonant launcher is interrupted by a set of slots to excite SWP in the CVD chamber. Next, we detail simulations and design of each part separately.

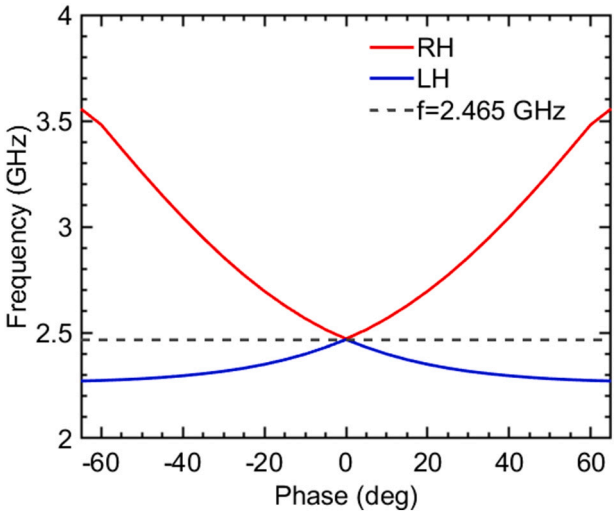

Fig. 2. Dispersion diagram of the unit cell showing RH (red) and LH (blue) wave propagation with infinite wavelength propagation frequency at 2.465 GHz (dashed line).

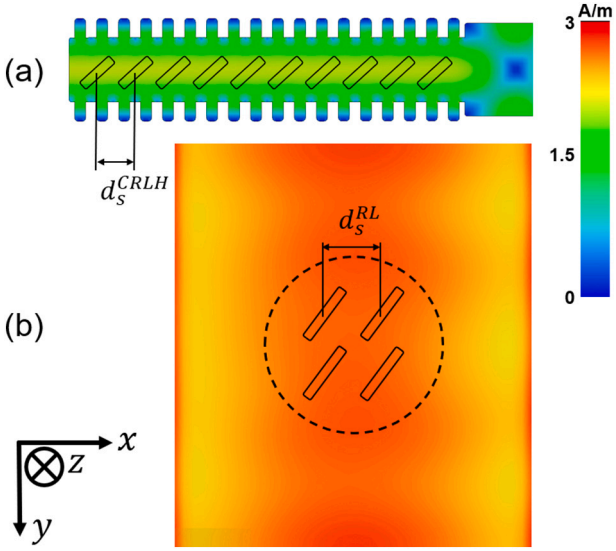

Fig. 3. Simulations results of the surface current density on (a) the shorted CRLH waveguide and (b) the resonant launcher. Black rectangles represent excitation slots while the dashed black circle indicates the position of the quartz window.

2.1. CRLH waveguide

The CRLH waveguide consists of a chain of periodically cascaded unit cells that support left-hand (LH) and right-hand (RH) wave propagation. Each unit cell is an artificial structure with a size in *x*-direction (see Fig. 1) much smaller than the wavelength of the guided wave, which can be represented by an equivalent circuit model as described in Ref. [34]. The CRLH waveguide supports infinite wavelength propagation only if all unit cells are balanced, meaning a unit cell does not have a

stop band and there is a seamless transition from LH to RH bands in the dispersion diagram. This criterion can be fulfilled by various designs of the unit cell as proposed in Refs. [35–38]. In this work we use a design of the unit cell similar to one presented in Ref. [38]. Fig. 2 shows the dispersion diagram of the chosen unit cell with infinite wavelength propagation frequency at 2.465 GHz that matches the frequency of the MW generator.

At infinite wavelength propagation frequency phase does not change as the wave propagates along the cells. Therefore, the surface current along the CRLH waveguide flows undisrupted and excitation slots can be placed at arbitrary positions with $d_s < \lambda_g/2$. We use a set of rectangular-shaped slots placed equidistant (d_s^{CRLH}=5 cm) along each CRLH waveguide. The finite integration method of Maxwell's equations is used to simulate surface currents on the CRLH waveguides and the resonant launcher. Fig. 3-(a) shows simulations results of the surface current density on the CRLH waveguide surface (*xy*-plane) coupled to the resonant launcher. All slots on the CRLH waveguide are excited either in phase or anti-phase. In total, four CRLH waveguides are used to couple MW radiation to the resonant launcher. Slots and the CRLH waveguides are placed in such a way that projection of magnetic current vector for each waveguide points in the same direction [39,40].

2.2. Resonant launcher

The resonant launcher is a resonant cavity placed below the array of CRLH waveguides. The size of the cavity is determined by the area occupied by the excitation slots with height chosen to be approximately half of the freespace wavelength (λ_0) at 2.465 GHz. The slots on CRLH waveguides couple MW radiation into the resonant launcher with the same direction of the magnetic current vector projection. As a result, the alternating magnetic field generates an electric field yielding a uniform surface current distribution over a large area [40]. Fig. 3-(b) shows simulations results of the surface current density on the resonant launcher surface (*xy*-plane), which faces the quartz window of the CVD chamber (see Fig. 1). Four slots placed equidistant from each other (d_s^{RL}=7 cm) are used to excite SWP in the CVD chamber. The length of each slot is chosen to be $\lambda_0/2$ making them resonant [41]. The 23 cm in diameter quartz window separates the resonant launcher from the CVD chamber. The quartz window and the resonant launcher are actively cooled by forced air flow. It is important to note that in this work we exploit only ≈30% of the available surface current area with one particular slot configuration for SWP excitation.

2.3. CVD chamber

The CVD chamber is a cylindrical, 21 cm in diameter, water-cooled resonant cavity equipped with the translational substrate holder. The electric field in the CVD chamber and in the rest of the system is simulated by solving Maxwell's equations in the frequency domain

$$\nabla \times \left(\mu_r^{-1} \nabla \times E\right) - \omega^2 \epsilon_0 \mu_0 \left(\epsilon_r - \frac{j\sigma}{\omega \epsilon_0}\right) E = 0, \quad (1)$$

where **E** is the electric field vector, ϵ_0 (μ_0) the permittivity (permeability) of free space, ω the angular frequency, σ the electrical conductivity and ϵ_r the relative permittivity. For simulation domains other than the CVD chamber we set ϵ_r=1 and σ=0. The SWP is assumed to be a cold collisional hydrogen plasma [42], which can be represented by a lossy isotropic dielectric with the permittivity and conductivity given by [43]

$$\epsilon_r = 1 - \frac{\omega_p^2}{\omega^2 + \nu_e^2} \text{ and } \sigma = \frac{\nu_e \epsilon_0 \omega_p^2}{\omega^2 + \nu_e^2}, \quad (2)$$

where ν_e is the electron-neutral collision frequency, $\omega_p = \sqrt{n_e e^2/m_e \epsilon_0}$ the plasma frequency, n_e the electron density, e the electron charge and m_e the electron mass. In a hydrogen discharge the collision frequency

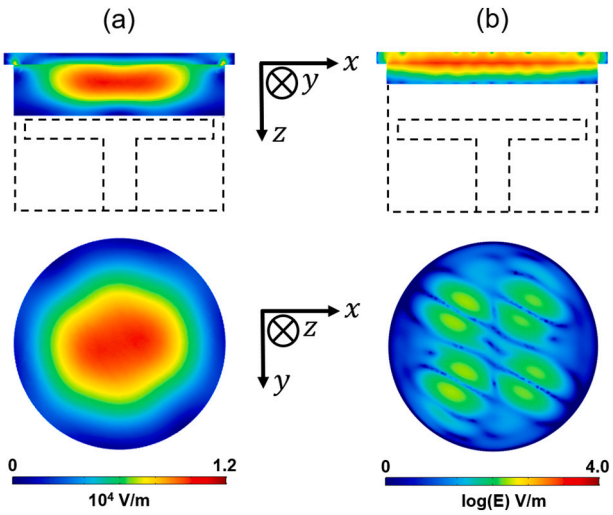

Fig. 4. Simulations results of the electric field in the CVD chamber for (a) pure hydrogen and (b) with SWP present. Cross sectional view in *xy*−plane shows results 2 cm away from the quartz window.

can be approximated as $\nu_e \approx 10^{12}(p/T_g)$ [44], where p is the gas pressure in mbar and T_g is the gas temperature in K. The pressure in simulations is set to the measured value (p=0.5 mbar) during the CVD process of NCD. The gas temperature at such pressure is close to room temperature due to the small kinetic energy transfer in elastic collisions between electrons and hydrogen atoms and is set to T_g= 300 K [45]. The electron density in SWP exceeds the cut-off density (n_c=7.4 × 10^{10} cm^{-3} at 2.45 GHz). The measured n_e values for hydrogen SWP close to the quartz window in slot-based systems are from 2 × 10^{11} cm^{-3} to 10^{12} cm^{-3} and falls rapidly with the distance [22,46]. Therefore, in simulations, we set the electron density to the experimentally measured value at p=0.5 mbar (n_e=5 × 10^{11} cm^{-3}) [46]. The MW field amplitude decays exponentially in SWP requiring fine mesh for the corresponding simulation region. Due to limited computational resources we exclude in the simulations the region where the distance between the quartz window and the substrate holder exceeds 2 cm. Fig. 4 shows electric field distributions in *xz*− and *xy*−planes for the CVD chamber simulated using the finite element analysis method for pure hydrogen case and with SWP present. In simulations the distance from the quartz window to the substrate holder is set to 51 mm yielding the total distance from the slots to the substrate holder of about $\lambda_0/2$. This constraint, similarly as for the resonant launcher, yields a uniform electric field distribution over large area as described in Ref. [40]. As a result, the chosen configuration of the slots on the resonant launcher and the constraint on the distance from the quartz window to the substrate holder, in the absence of the gas discharge, yields similar electric field strength over a deposition area enabling the covering of a 4-inch Si wafer as illustrated in Fig. 4(a). In the presence of the SWP, however, the electron density is $n_e > n_c$ and MW propagate as a surface wave along the quartz-plasma interface. Excited surface waves from adjacent slots interact with each other yielding a standing surface wave pattern. Due to the chosen configuration of the slots the wave field is homogeneously distributed over the deposition area as shown in Fig. 4(b). This yields a uniform plasma distribution, witch is further confirmed by experimental results presented in the next sections. The electric field strength decays rapidly with the distance from the quartz window indicating that MW power absorption by plasma close to the quartz-plasma interface is the highest. In experiments, a plasma diffuses from a quartz window towards a substrate with a falling density. Typically, for diamond synthesis with SWP the substrate is placed in the so called "CVD region", which starts approximately at 4.5 cm away from the quartz window and extends up to 20 cm [46].

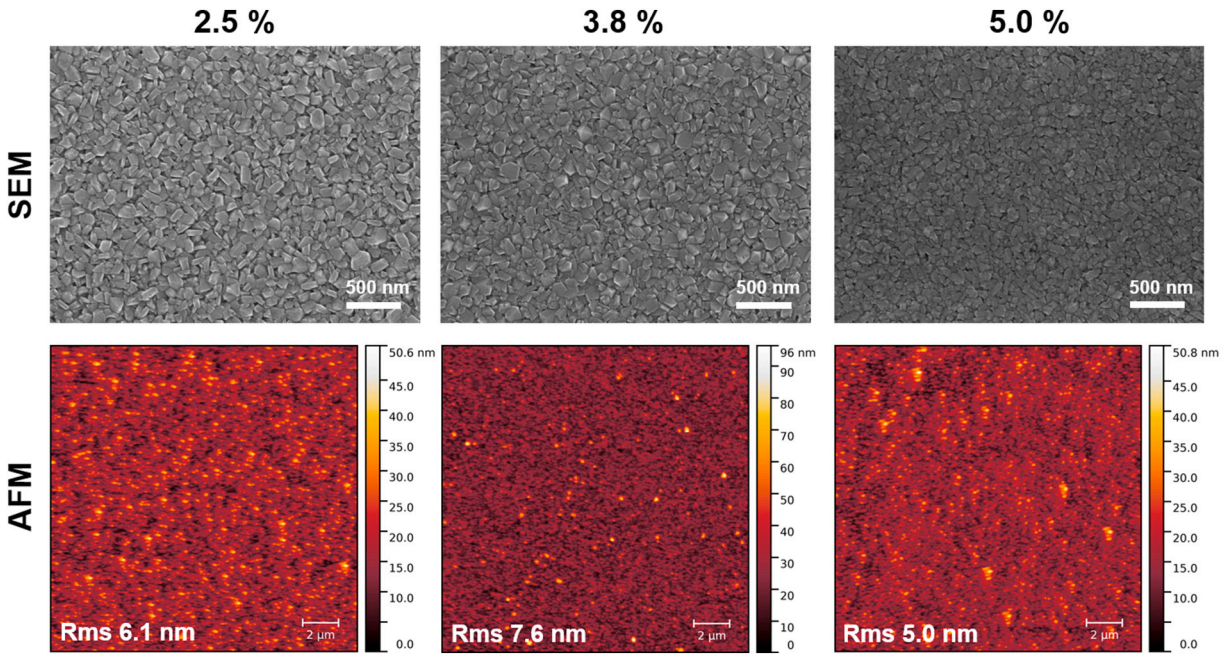

Fig. 5. SEM and AFM images of NCD films grown with 2.5 %, 3.8 % and 5.0 % CH_4 concentration in $H_2/CH_4/CO_2$ gas mixture.

It is worth noting that other configurations of slots (size, shape, placement, etc.) can be used for SWP excitation. Plasma uniformity could also be further improved by using a corrugated dielectric plate [42,47] instead of the quartz window. Lastly, CRLH waveguides alone could be used as SWP sources avoiding use of the resonant launcher.

3. Experimental

The NCD films were grown on polished (100) oriented 4-inch Si wafers with thickness of 525 μm. All samples were grown with the new in-house built SWP MWPECVD system at the same MW power of 2 kW keeping constant 0.5 mbar process pressure. The $H_2/CH_4/CO_2$ gas mixture was used with the CO_2 fraction fixed to 10 % while CH_4 concentration was varied from 2.5 % to 5.0 %. The total gas flow was 78 sccm and the growth time was 2 h for all samples. The Si substrates were placed on the molybdenum holder 51 mm away from the quartz window keeping the same distance as in the simulations described above (see Fig. 4). The substrate holder was not additionally heated apart from the diffusive plasma. The temperature was measured with type K thermocouple embedded in the molybdenum holder.

Prior to growth the substrates were seeded with 5–7 nm size nanodiamonds (ND). To nucleate the Si wafer with ND seeds a water-based ND colloid was drop-cast onto the sample surface covering it completely. Then followed by spinning the wafer at 2000 rpm and flushing it with deionized water for 30 s, and finally leaving it spinning for 60 s till the surface dries [48,49]. This yields seeding density of approximately 4×10^{11} cm^{-2}.

Surface morphology and roughness of the NCD films were investigated by scanning electron microscopy (SEM, Raith e-Line), using an inlens detector and an acceleration voltage of 10 kV, and atomic force microscopy (AFM, Anfatec, Eddy) operated in contact mode using a MicroMash CSC17 cantilever. The film thicknesses were measured using spectral reflectance technique (Filmetrics F10-RT). The Raman spectra were measured with HORIBA LabRAM 800 HR spectrometer working in a confocal mode and using 488 nm wavelength Ar laser as an excitation source.

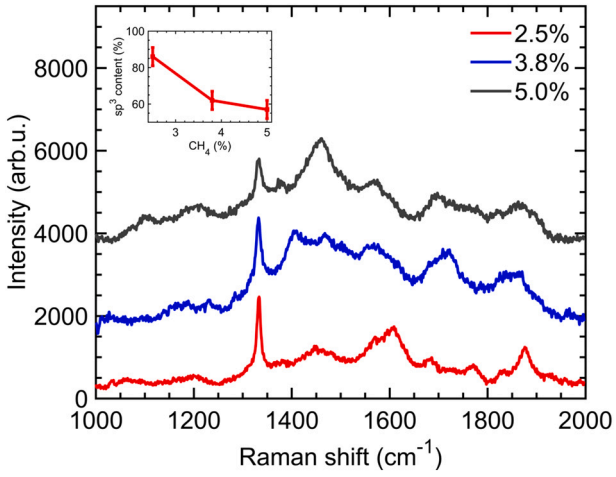

Fig. 6. Background corrected Raman spectra of NCD films grown with 2.5 % (red line), 3.8 % (blue line) and 5.0 % (black line) CH_4 concentration. Spectra lines are shifted vertically for illustrative purposes. The inset shows sp^3 content as a function of CH_4 concentration.

4. Results and discussion

We varied the CH_4 concentration in the $H_2/CH_4/CO_2$ gas mixture to investigate changes in NCD films morphology, structure and growth rates. Fig. 5 shows SEM and AFM images of NCD film surfaces of three samples grown using 2.5 %, 3.8 % and 5.0 % CH_4 concentration at 410 °*C*, 395 °*C* and 405 °*C* temperature, respectively. The grain sizes are similar in size for all the films. The root-mean-square (rms) roughness of the surface was measured on several spots for each of the sample and ranges from 5 nm to 10 nm. The increase in CH_4 concentration from 2.5 % to 5.0 % does not induce significant changes of NCD film surface morphology.

Fig. 6 shows measured and background corrected Raman spectra for the three samples mentioned above. The characteristic diamond peak is observed at 1332 cm^{-1} and a broad line shape is visible around 1580 cm^{-1} corresponding to D and G bands, respectively. The broad peaks

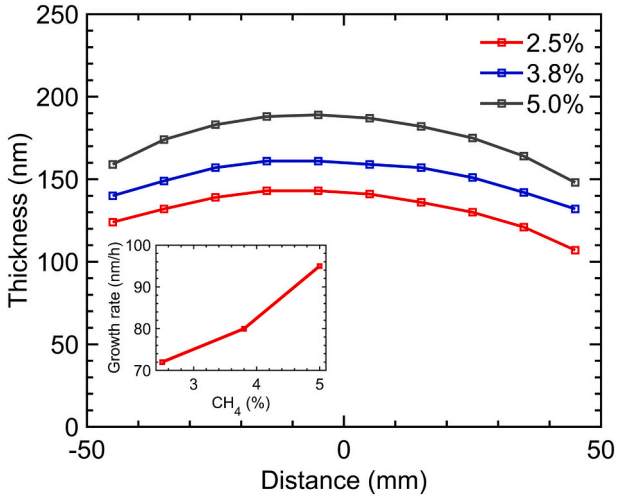

Fig. 7. Thickness profiles of NCD films grown with 2.5 % (red line), 3.8 % (blue line) and 5.0 % (black line) CH_4 concentration. The inset shows growth rate as a function of CH_4 concentration.

near 1190 cm^{-1} and 1480 cm^{-1} assigned to transpolyacetylene segments at grain boundaries [50–52] are clearly visible for sample grown with 5.0 % CH_4 concentration representing a signature of NCD. The amount of sp^3 bonded carbon was calculated using formula [53–58]:

$$sp^3 = \frac{75 \times I_d}{75 \times I_d + \sum I_{nd}}, \quad (3)$$

where I_d is the integrated diamond peak intensity (at 1332 cm^{-1}), I_{nd} is the integrated non-diamond peak intensity. The diamond signal efficiency factor of 75 was used, because sp^2 and sp^3 bonded carbon have different sensitivity to the laser excitation [59–62]. The amount of sp^3 bonded carbon in NCD films is estimated to be 83%, 62% and 57% for 2.5 %, 3.8 % and 5.0 % CH_4 concentration, respectively.

Fig. 7 shows thickness profiles of the NCD films measured across the center of 4-inch Si wafers. The variation of the film thickness for all samples ranges on average from 15% to 19%. The thickness variation can be further decreased by using a larger CVD chamber and increasing the number of excitation slots. The growth rate increases with increasing CH_4 concentration and is, measured at the center of the wafer, 72 nm/h, 80 nm/h and 95 nm/h for 2.5 %, 3.8 % and 5.0 % CH_4 concentrations, respectively. We expect that the growth rate can be further improved in the new SWP MWPECVD system by varying process pressure, increasing substrate temperature or reducing substrate distance from the quartz window.

5. Conclusion

In this work, a novel method to excite SWP, based on unique properties of metamaterials, for growth of NCD has been presented. The method uses infinite wavelength propagation of CRLH waveguides to induce large area surface currents on the resonant launcher. This unique feature allows arbitrary placement of the excitation slots yielding uniform SWP distribution. Further scaling-up of the SWP can be easily achieved by increasing the size of the CVD chamber and the number of the excitation slots.

The new SWP MWPECVD system has been used to demonstrate the growth of diamond on 4-inch Si wafers. The $H_2/CH_4/CO_2$ gas mixture has been used to grow low surface roughness (5–10 nm) NCD films at low temperatures (395 °C - 410 °C) with growth rates reaching up to 95 nm/h. The NCD films exhibit high sp^3 content and have thickness variation less than 19%.

CRediT authorship contribution statement

Justas Zalieckas: Conceptualization, Methodology, Investigation, Writing - Original Draft. **Paulius Pobedinskas:** Formal analysis, Investigation, Writing - Review & Editing. **Martin Møller Greve:** Formal analysis, Investigation, Writing - Review & Editing. **Kristoffer Eikehaug:** Investigation, Resources. **Ken Haenen:** Writing - Review & Editing. **Bodil Holst:** Writing - Review & Editing.

Declaration of competing interest

The authors declare that they have no known competing financial interests or personal relationships that could have appeared to influence the work reported in this paper.

Acknowledgments

This work was financially supported by the FORNY programme under the Research Council of Norway and the Methusalem NANO network.

References

[1] O. Auciello, A.V. Sumant, Status review of the science and technology of ultrananocrystalline diamond (uncd) films and application to multifunctional devices, Diam. Relat. Mater. 19 (7) (2010) 699–718, https://doi.org/10.1016/j.diamond.2010.03.015.
[2] A.V. Sumant, O. Auciello, R.W. Carpick, S. Srinivasan, J.E. Butler, Ultrananocrystalline and nanocrystalline diamond thin films for mems/nems applications, MRS Bull. 35 (4) (2010) 281–288, https://doi.org/10.1557/mrs2010.550.
[3] J. Rubio-Retama, J. Hernando, B. López-Ruiz, A. Härtl, D. Steinmüller, M. Stutzmann, E. López-Cabarcos, J. Antonio Garrido, Synthetic nanocrystalline diamond as a third-generation biosensor support, Langmuir 22 (13) (2006) 5837–5842, https://doi.org/10.1021/la060167r.
[4] D. Nidzworski, K. Siuzdak, P. Niedziałkowski, R. Bogdanowicz, M. Sobaszek, J. Ryl, P. Weiher, M. Sawczak, E. Wnuk, W.A. Goddard, A. Jaramillo-Botero, T. Ossowski, A rapid-response ultrasensitive biosensor for influenza virus detection using antibody modified boron-doped diamond, Sci. Rep. 7 (1) (2017) 15707, https://doi.org/10.1038/s41598-017-15806-7.
[5] H. Liu, D.S. Dandy, Diamond Chemical Vapor Deposition, William Andrew Publishing, 1995.
[6] Edited by R. Narayan, Diamond-Based Materials for Biomedical Applications, Woodhead Publishing Series in Biomaterials, 2013.
[7] F. Silva, K. Hassouni, X. Bonnin, A. Gicquel, Microwave engineering of plasma-assisted cvd reactors for diamond deposition, J. Phys. Condens. Matter 21 (36) (2009) 364202, https://doi.org/10.1088/0953-8984/21/36/364202.
[8] J.J. Gracio, Q.H. Fan, J.C. Madaleno, Diamond growth by chemical vapour deposition, J. Phys. D. Appl. Phys. 43 (37) (2010) 374017, https://doi.org/10.1088/0022-3727/43/37/374017.
[9] M. Ihara, H. Maeno, K. Miyamoto, H. Komiyama, Low-temperature deposition of diamond in a temperature range from 70 c to 700 c, Diam. Relat. Mater. 1 (2) (1992) 187–190, https://doi.org/10.1016/0925-9635(92)90022-G.
[10] F. Piazza, G. Morell, Synthesis of diamond at sub 300 c substrate temperature, Diam. Relat. Mater. 16 (11) (2007) 1950–1957, https://doi.org/10.1016/j.diamond.2007.08.038.
[11] Y. Liou, A. Inspektor, R. Weimer, R. Messier, Low-temperature diamond deposition by microwave plasma-enhanced chemical vapor deposition, Appl. Phys. Lett. 55 (7) (1989) 631–633, https://doi.org/10.1063/1.101807.
[12] J. Lee, R.W. Collins, R. Messier, Y.E. Strausser, Low temperature plasma process based on co-rich co/h_2 mixtures for high rate diamond film deposition, Appl. Phys. Lett. 70 (12) (1997) 1527–1529, https://doi.org/10.1063/1.118607.
[13] J.R. Petherbridge, P.W. May, S.R.J. Pearce, K.N. Rosser, M.N.R. Ashfold, Low temperature diamond growth using co_2/ch_4 plasmas: molecular beam mass spectrometry and computer simulation investigations, J. Appl. Phys. 89 (2) (2001) 1484–1492, https://doi.org/10.1063/1.1333031.
[14] L. Wang, Y. Wang, J. Zhou, S. Ouyang, Diamond films produced by microwave plasma chemical vapor deposition at low temperature and their characterization, Mater. Sci. Eng. A 475 (1) (2008) 17–19, https://doi.org/10.1016/j.msea.2006.12.139.
[15] A. Hiraki, Low-temperature (200 c) growth of diamond on nano-seeded substrates, Appl. Surf. Sci. 162-163 (2000) 326–331, https://doi.org/10.1016/S0169-4332(00)00211-7.
[16] H.-A. Mehedi, J. Achard, D. Rats, O. Brinza, A. Tallaire, V. Mille, F. Silva, C. Provent, A. Gicquel, Low temperature and large area deposition of nanocrystalline diamond films with distributed antenna array microwave-plasma reactor, Diam. Relat. Mater. 47 (2014) 58–65, https://doi.org/10.1016/j.diamond.2014.05.004.

[17] B. Baudrillart, F. Bénédic, A. S. Melouani, F. J. Oliveira, R. F. Silva, J. Achard, Low-temperature deposition of nanocrystalline diamond films on silicon nitride substrates using distributed antenna array pecvd system, Physica Status Solidi (A) 213 (10) (2016) 2575–2581. doi:https://doi.org/10.1002/pssa.201600221.

[18] K. Tsugawa, M. Ishihara, J. Kim, M. Hasegawa, Y. Koga, Large area and low temperature nanodiamond coating by microwave plasma chemical vapor deposition, New Diamond and Frontier Carbon Technology 16 (2007) 337–346.

[19] J. Kim, K. Tsugawa, M. Ishihara, Y. Koga, M. Hasegawa, Large-area surface wave plasmas using microwave multi-slot antennas for nanocrystalline diamond film deposition, Plasma Sources Sci. Technol. 19 (1) (2009), 015003, https://doi.org/10.1088/0963-0252/19/1/015003.

[20] K. Tsugawa, M. Ishihara, J. Kim, Y. Koga, M. Hasegawa, Nucleation enhancement of nanocrystalline diamond growth at low substrate temperatures by adamantane seeding, J. Phys. Chem. C 114 (9) (2010) 3822–3824, https://doi.org/10.1021/jp910555x.

[21] T. Izak, O. Babchenko, M. Varga, S. Potocky, A. Kromka, Low temperature diamond growth by linear antenna plasma cvd over large area, Physica Status Solidi (B) 249 (12) (2012) 2600–2603. doi:https://doi.org/10.1002/pssb.201200103.

[22] K. Tsugawa, M. Ishihara, J. Kim, Y. Koga, M. Hasegawa, Nanocrystalline diamond film growth on plastic substrates at temperatures below 100 c from low-temperature plasma, Phys. Rev. B 82 (2010) 125460, https://doi.org/10.1103/PhysRevB.82.125460.

[23] L. Latrasse, A. Lacoste, J. Sirou, J. Pelletier, High density distributed microwave plasma sources in a matrix configuration: concept, design and performance, Plasma Sources Sci. Technol. 16 (1) (2006) 7–12, https://doi.org/10.1088/0963-0252/16/1/002.

[24] J. Pollak, M. Moisan, Z. Zakrzewski, J. Pelletier, Y.A. Arnal, A. Lacoste, T. Lagarde, Compact waveguide-based power divider feeding independently any number of coaxial lines, IEEE Transactions on Microwave Theory and Techniques 55 (5) (2007) 951–957, https://doi.org/10.1109/TMTT.2007.895643.

[25] A. Kromka, O. Babchenko, T. Izak, K. Hruska, B. Rezek, Linear antenna microwave plasma cvd deposition of diamond films over large areas, Vacuum 86 (6) (2012) 776–779, https://doi.org/10.1016/j.vacuum.2011.07.008.

[26] M. Nagatsu, K. Naito, A. Ogino, S. Nanko, Production of large-area surface-wave plasmas with an internally mounted planar cylindrical launcher, Plasma Sources Sci. Technol. 15 (1) (2005) 37–41, https://doi.org/10.1088/0963-0252/15/1/006.

[27] X. Chang, K. Kunii, R. Liang, M. Nagatsu, Study of cavity type antenna structure of large-area 915 mhz ultra-high frequency wave plasma device based on three-dimensional finite difference time-domain analysis, J. Appl. Phys. 114 (18) (2013) 183302, https://doi.org/10.1063/1.4831656.

[28] T.J. Wu, C.S. Kou, A large-area plasma source excited by a tunable surface wave cavity, Rev. Sci. Instrum. 70 (5) (1999) 2331–2337, https://doi.org/10.1063/1.1149759.

[29] M. Liehr, S. Wieder, M. Dieguez-Campo, Large area microwave coating technology, Thin Solid Films 502 (1) (2006) 9–14, https://doi.org/10.1016/j.tsf.2005.07.226.

[30] S. Drijkoningen, P. Pobedinskas, S. Korneychuk, A. Momot, Y. Balasubramaniam, M.K. Van Bael, S. Turner, J. Verbeeck, M. Nesládek, K. Haenen, On the origin of diamond plates deposited at low temperature, Cryst. Growth Des. 17 (8) (2017) 4306–4314, https://doi.org/10.1021/acs.cgd.7b00623.

[31] A. Taylor, P. Ashcheulov, P. Hubík, L. Klimša, J. Kopeček, Z. Remeš, Z. Vlčková Živcová, M. Remzová, L. Kavan, E. Scheid, J. Lorinčík, V. Mortet, Precursor gas composition optimisation for large area boron doped nano-crystalline diamond growth by mw-la-pecvd, Carbon 128 (2018) 164–171, https://doi.org/10.1016/j.carbon.2017.11.063.

[32] N. Suzuki, H. Kitagawa, S. Uchiyama, Stable surface-wave plasma through excitation of standing surface wave using plane multislot antenna, Japanese Journal of Applied Physics 41 (Part 1, No. 6A) (2002) 3930–3935. doi:https://doi.org/10.1143/jjap.41.3930.

[33] Z. Zakrzewski, M. Moisan, Plasma sources using long linear microwave field applicators: main features, classification and modelling, Plasma Sources Sci. Technol. 4 (3) (1995) 379–397, https://doi.org/10.1088/0963-0252/4/3/008.

[34] A. Lai, T. Itoh, C. Caloz, Composite right/left-handed transmission line metamaterials, IEEE Microw. Mag. 5 (3) (2004) 34–50, https://doi.org/10.1109/MMW.2004.1337766.

[35] A. M. N. Eldeen, I. A. Eshrah, Crlh waveguide with air-filled double-ridge corrugations, in: 2011 IEEE International Symposium on Antennas and Propagation (APSURSI), 2011 IEEE International Symposium on Antennas and Propagation (APSURSI), 2011, pp. 2965–2968. doi:https://doi.org/10.1109/APS.2011.5997151.

[36] T. Ueda, N. Michishita, M. Akiyama, T. Itoh, Dielectric-resonator-based composite right/left-handed transmission lines and their application to leaky wave antenna, IEEE Transactions on Microwave Theory and Techniques 56 (10) (2008) 2259–2269, https://doi.org/10.1109/TMTT.2008.2003524.

[37] L. Shaowei, Y. Ping, X. Jianhua, W. Ya, Left-handed transmission line based on resonant-slot coupled cavity chain, IEEE Microwave and Wireless Components Letters 17 (4) (2007) 292–294, https://doi.org/10.1109/LMWC.2007.892982.

[38] Y. Chen, S.W. Liao, J. Wei, J.H. Xu, Unequally spaced and excited resonant slotted-waveguide antenna array based on an improved resonant-slot coupled cavity chain composite right/left-handed waveguide, Prog. Electromagn. Res. 110 (2010) 421–435, https://doi.org/10.2528/PIER10101905.

[39] S. Liao, J. Wang, Y. Chen, W. Tang, J. Wei, J. Xu, Z. Zhao, Synthesis, simulation and experiment of unequally spaced resonant slotted-waveguide antenna arrays based on the infinite wavelength propagation property of composite right/left-handed waveguide, IEEE Trans. Antennas Propag. 60 (7) (2012) 3182–3194, https://doi.org/10.1109/TAP.2012.2196922.

[40] J. Zalieckas, Large area microwave plasma chemical vapour deposition (la mpcvd) reactor apparatus and method for providing same (Norwegian. Pat. Nr. 345052 (2020)).

[41] G. Sauvé, M. Moisan, Z. Zakrzewski, Slotted waveguide field applicator for the generation of long uniform plasmas, J. Microw. Power Electromagn. Energy. 28 (3) (1993) 123–131, https://doi.org/10.1080/08327823.1993.11688214.

[42] E. Abdel Fattah, I. Ganachev, H. Sugai, Numerical 3d simulation of surface wave excitation in planar-type plasma processing device with a corrugated dielectric plate, Vacuum 86 (3) (2011) 330–334, https://doi.org/10.1016/j.vacuum.2011.07.058.

[43] M. Füner, C. Wild, P. Koidl, Numerical simulations of microwave plasma reactors for diamond cvd, Surf. Coat. Technol. 74-75 (1995) 221–226, https://doi.org/10.1016/0257-8972(95)08232-8.

[44] W. Tan, T.A. Grotjohn, Modeling the electromagnetic excitation of a microwave cavity plasma reactor, J. Vac. Sci. Technol. A 12 (4) (1994) 1216–1220, https://doi.org/10.1116/1.579298.

[45] A. Palmero, J. Cotrino, C. Lao, A. Barranco, A. R. González-Elipe, Gas temperature measurement in a surface-wave argon plasma column at low pressures, Japanese Journal of Applied Physics 41 (Part 1, No. 9) (2002) 5787–5791. doi:https://doi.org/10.1143/jjap.41.5787.

[46] K. Tsugawa, S. Kawaki, M. Ishihara, J. Kim, Y. Koga, H. Sakakita, H. Koguchi, M. Hasegawa, Nanocrystalline diamond growth in a surface-wave plasma, Diam. Relat. Mater. 20 (5) (2011) 833–838, https://doi.org/10.1016/j.diamond.2011.03.031.

[47] T. Yamauchi, E. Abdel-Fattah, H. Sugai, Dramatic improvement of surface wave plasma performance using a corrugated dielectric plate, Japanese Journal of Applied Physics 40 (Part 2, No. 11A) (2001) L1176–L1178. doi:https://doi.org/10.1143/jjap.40.l1176.

[48] P. Pobedinskas, G. Degutis, W. Dexters, J. D'Haen, M.K. Van Bael, K. Haenen, Nanodiamond seeding on plasma-treated tantalum thin films and the role of surface contamination, Appl. Surf. Sci. 538 (2021) 148016, https://doi.org/10.1016/j.apsusc.2020.148016.

[49] G. Degutis, P. Pobedinskas, H.-G. Boyen, W. Dexters, W. Janssen, S. Drijkoningen, A. Hardy, K. Haenen, M.K. Van Bael, Improved nanodiamond seeding on chromium by surface plasma pretreatment, Chem. Phys. Lett. 640 (2015) 50–54, https://doi.org/10.1016/j.cplett.2015.10.002.

[50] C. Mapelli, C. Castiglioni, G. Zerbi, K. Müllen, Common force field for graphite and polycyclic aromatic hydrocarbons, Phys. Rev. B 60 (1999) 12710–12725, https://doi.org/10.1103/PhysRevB.60.12710.

[51] A.C. Ferrari, J. Robertson, Origin of the 1150 − cm^{-1} Raman mode in nanocrystalline diamond, Phys. Rev. B 63 (2001) 121405, https://doi.org/10.1103/PhysRevB.63.121405.

[52] R. Pfeiffer, H. Kuzmany, P. Knoll, S. Bokova, N. Salk, B. Günther, Evidence for trans-polyacetylene in nano-crystalline diamond films, Diam. Relat. Mater. 12 (3) (2003) 268–271, https://doi.org/10.1016/S0925-9635(02)00336-9.

[53] W. Fortunato, A. J. Chiquito, J. C. Galzerani, J. R. Moro, Crystalline quality and phase purity of cvd diamond films studied by raman spectroscopy, J. Mater. Sci. 42 (2007) 7331â€“7336. doi:https://doi.org/10.1007/s10853-007-1575-0.

[54] R. Loudon, The Raman effect in crystals, Adv. Phys. 13 (52) (1964) 423–482, https://doi.org/10.1080/00018736400101051.

[55] N. Wada, S. A. Solin, Raman efficiency measurements of graphite, Physica B+C 105 (1) (1981) 353–356. doi:https://doi.org/10.1016/0378-4363(81)90274-6.

[56] R.E. Shroder, R.J. Nemanich, J.T. Glass, Analysis of the composite structures in diamond thin films by Raman spectroscopy, Phys. Rev. B 41 (1990) 3738–3745, https://doi.org/10.1103/PhysRevB.41.3738.

[57] F. Silva, A. Gicquel, A. Tardieu, P. Cledat, T. Chauveau, Control of an MPACVD reactor for polycrystalline textured diamond films synthesis: role of microwave power density, Diam. Relat. Mater. 5 (3) (1996) 338–344, https://doi.org/10.1016/0925-9635(95)00428-9.

[58] D. Ballutaud, F. Jomard, T. Kociniewski, E. Rzepka, H. Girard, S. Saada, Sp3/sp2 character of the carbon and hydrogen configuration in micro- and nanocrystalline diamond, Diam. Relat. Mater. 17 (4) (2008) 451–456, https://doi.org/10.1016/j.diamond.2007.10.004.

[59] J. Wagner, C. Wild, P. Koidl, Resonance effects in Raman scattering from polycrystalline diamond films, Appl. Phys. Lett. 59 (7) (1991) 779–781, https://doi.org/10.1063/1.105340.

[60] S. Leeds, T. Davis, P. May, C. Pickard, M. Ashfold, Use of different excitation wavelengths for the analysis of CVD diamond by laser Raman spectroscopy, Diam. Relat. Mater. 7 (2) (1998) 233–237, https://doi.org/10.1016/S0925-9635(97)00261-6.

[61] A.C. Ferrari, J. Robertson, Resonant Raman spectroscopy of disordered, amorphous, and diamondlike carbon, Phys. Rev. B 64 (2001), 075414, https://doi.org/10.1103/PhysRevB.64.075414.

[62] E. L. H. Thomas, S. Mandal, Ashek-I-Ahmed, J. E. Macdonald, T. G. Dane, J. Rawle, C.-L. Cheng, O. A. Williams, Spectroscopic ellipsometry of nanocrystalline diamond film growth, ACS Omega 2 (10) (2017) 6715–6727. doi:https://doi.org/10.1021/acsomega.7b00866.